# 15

# Dynamic seasonal prediction and predictability of the monsoon

*In-Sik Kang and Jagadish Shukla*

In this chapter we present a historical review of the hypothesis of boundary forced predictability of the monsoon and the limitations and challenges in dynamical seasonal prediction of monsoon rainfall. We also present an assessment of multi-model seasonal predictability of summer mean precipitation over the Asian monsoon–western Pacific region by using a set of 21-year (1979–1999) hindcast predictions of 5 models participating at the Asia–Pacific Economic Cooperation Climate Network (APCN). The five models consist of the current operational seasonal prediction models of NCEP, NASA, JMA, KMA, and SNU. The potential predictabilities of individual models are shown by various methods including the signal-to-noise ratio and anomaly correlations. Statistical methods for correcting the bias of model prediction are developed and applied to individual model predictions. We demonstrate that statistical correction is effective for enhancing the predictability, particularly for the Asian monsoon–Pacific region, where the models have a large bias. It is shown that a reasonably good seasonal prediction can be achieved when multimodel predictions are combined based on a composite of the individual predictions, after applying a statistical correction to each of them separately.

Although this chapter describes mainly the current status of tier-2 seasonal prediction systems, the present skills of tier-1 systems, utilizing coupled ocean–atmosphere models are also examined using the data from the Development of a European Multimodel Ensemble System for seasonal to inTERannual prediction (DEMETER). We show that the tier-1 system has an advantage in producing better seasonal mean predictions, particularly in the western Pacific and Indian Ocean where air–sea interaction is active during the summer. The spatial correlation skill of the DEMETER multimodel ensemble prediction is 0.47 for monsoon precipitation over the region of 40–180°E, 20°S–30°N.

B. Wang (ed.), *The Asian Monsoon*.

## 15.1 INTRODUCTION

### 15.1.1 Historical review

Variations in monsoon rainfall affect agriculture, drinking water, transportation, health, power, and the very livelihood of billions of people living in the monsoon region. It is no surprise therefore that for over a hundred years a number of countries in the region have tried to issue long-range forecasts of monsoons (The India Meteorological Department started issuing long-range forecasts of monsoon rainfall in 1886). The operational long-range forecasts of monsoon rainfall were based on empirical relationships derived from past observations of atmospheric pressure, temperature, and wind. Blanford (1884) was the first to suggest the use of a surface boundary condition (snowfall over the Himalayas in the preceding winter) to predict the summer monsoon rainfall over India.

Charney and Shukla (1981) presented a conceptual hypothesis of monsoon predictability based on the influence of boundary forcing at the Earth's surface. A brief historical perspective on this hypothesis is given here. Charney *et al.* (1977) had conducted atmospheric general circulation model (AGCM) experiments with the NASA/GISS AGCM to investigate the influence of changes in albedo on rainfall over the Sahel. In these experiments it was found that the summer rainfall variance among the three ensemble members (each member was integrated only for 45 days) was quite small over the Indian monsoon region, indicating that the boundary conditions mainly control the Indian monsoon rainfall. In the same year, Shukla and Misra (1977) had shown empirical evidence of a possible relationship between the Arabian Sea surface temperature (SST) and Indian rainfall, and Shukla (1975) had shown that in the Geophysical Fluid Dynamics Laboratory (GFDL) AGCM, specification of (large) positive SST anomalies over the Arabian Sea produced an increase in monsoon rainfall over India. Hahn and Shukla (1976) revived Blanford's hypothesis of a snow–monsoon relationship by showing, using satellite derived snow cover data, an inverse relationship between the winter season snow cover over Eurasia and the subsequent summer monsoon rainfall over India. These results, combined with the results from the GISS model, in which variance of seasonal rainfall among ensemble members was quite small, led Charney and Shukla (1981) to hypothesize that the predictability of the monsoon depends on the influence of boundary conditions at the Earth's surface.

The Charney–Shukla hypothesis has been the central paradigm for monsoon predictability research during the past 25 years. However, dynamical models have included large systematic errors in their simulations of the seasonal mean anomalies associated with changes in boundary conditions, and therefore their predictability for summer monsoon rainfall has been relatively low. Whether our inability to capture the boundary forced signals is due to inadequate models and modeling strategies or due to intrinsic limits to the predictability of seasonal mean rainfall because of the large natural intraseasonal variability of monsoons remains an open question and a topic of vigorous debate. In the following section we present a critical

retrospective of the Charney–Shukla hypothesis and describe the barriers to realizing its potential predictability.

For the boundary conditions to have a useful influence on the prediction of monsoon rainfall, the following three conditions need to be satisfied: (1) there must be a large and persistent anomaly at the Earth's surface, (2) there must be a well defined dynamical mechanism through which changes in the boundary conditions will produce a corresponding change in the seasonal mean monsoon rainfall, and (3) the seasonal mean response (signal) must be sufficiently large and reproducible so that it can be distinguished from the intrinsic variability (noise) of the model due to internal dynamics alone. A large number of model simulations during the past decade with high-resolution AGCMs using advanced parameterizations have clearly shown that the internal variability over the monsoon region is much larger than that found by Charney and Shukla. This implies that large member ensembles are needed to distinguish the boundary forced response from internal dynamics variability. If the internal variability is spatially small-scale and high-frequency, then large-scale spatio–temporal averages (viz. the seasonal mean over the whole of India) could be predicted if the boundary forcings were indeed important, and if the models were able to simulate the appropriate physical effects.

The current generation of AGCMs have such large systematic errors in simulating both the mean and the variance of summer monsoon rainfall that it is not possible to conclude whether our current inability to make useful dynamical seasonal prediction is due to the lack of boundary forced predictability or the inadequacy of the current models and modeling strategies. Recent research works carried out with coupled ocean–atmosphere models, suggest that the prescription of SST anomalies in AGCM experiments is an inadequate modeling strategy because SST anomalies in the Indian Ocean and the adjoining western Pacific Ocean are either forced by the atmosphere or evolve as a strongly coupled ocean–atmosphere process (Wang *et al.*, 2004a). If ocean–atmosphere coupling is indeed crucial for the Indian Ocean and western Pacific SST anomalies, the predictability of monsoons must be investigated with coupled ocean–atmosphere models, which currently have large systematic errors. The problem is further compounded by the fact that atmosphere–land interactions are also quite important for the simulation and prediction of monsoon rainfall. Even if SST anomalies force significant changes in large-scale circulation, local land–atmosphere interactions will modulate the ocean-forced remote response and determine the actual changes in rainfall over land. Therefore, realistic models of the total climate system (ocean–land–atmosphere) are required to understand the variability and to make useful predictions of monsoon rainfall.

### 15.1.2 Current dynamic seasonal predictions

In spite of the many challenges described above, dynamic seasonal predictions using general circulation models (GCMs) have been implemented by several operational centers in recent years. In particular, possible improvement of seasonal prediction has been attempted with the use of multimodel ensembles to remove the uncertainties

associated with the spread of ensemble predictions with different initial conditions and the uncertainties associated with model parameterizations (Krishnamurti *et al.*, 1999; Palmer *et al.*, 2004). This chapter describes the present status of dynamical multimodel ensemble seasonal prediction systems, particularly for the monsoon precipitation.

In an ensemble simulation, all ensemble members are forced by the same SST but start from slightly different atmospheric initial conditions (Dix and Hunt, 1995; Kumar and Hoerling, 1995; Stern and Miyakoda, 1995; Zwiers, 1996; Kang *et al.*, 2004). The basic idea of this approach is that the differences among the ensemble members can be used to quantify the noise due to internal dynamics, whereas the relative similarity between ensemble members can be considered as the atmospheric response to external forcing. Thus, the ensemble mean (signal) can be considered as the component of the prediction forced by the SST, and the deviation from the ensemble mean as the stochastic internal component of the prediction. In this approach, the potential predictability is measured as the ratio between the externally forced SST signal and the internal noise, using a standard statistical tool for this kind of problem: 'analysis of variance' (ANOVA), which has been detailed in many previous studies (Shukla, 1981; Rowell *et al.*, 1995; Rowell, 1998).

Recently, attempts have also been made to reduce the uncertainty of models by simply compositing multimodel solutions (Kang *et al.*, 2002) or by using the so-called 'superensemble' method (Krishnamurti *et al.*, 1999). The present performance of dynamical seasonal prediction is poor, unless some form of post-processing is applied. This poor performance is not only due to the inherent complexity of atmospheric internal processes but also due to the present models' inability to reproduce the actual atmospheric responses to external forcings, particularly the SST anomalies. This model bias in the external component arises from imperfect formulation and parameterization of the various physical processes in the model. Different parameterizations produce different solutions. Assuming that the errors of those solutions are independent of each other and that various model solutions spread randomly but close to the observation are used, the composite of many model solutions can reduce the random errors of the models.

Model error can also be reduced by statistical correction methods. A major part of the non-system error of each model can be corrected by incorporating a statistical relationship between the predicted and observed anomalies. The most commonly used methodology is the so-called coupled pattern technique (Graham *et al.*, 1994), based on singular value decomposition (SVD) analysis and canonical correlation analysis (CCA). Ward and Navarra (1997) applied SVD to simultaneous fields of GCM simulated precipitation and observed precipitation to correct the errors in the model response to SST forcing. CCA has been widely used in a statistical seasonal prediction system (Barnett and Preisendorfer, 1987; Barnston, 1994). A recent study by Feddersen *et al.* (1999) demonstrated that post-processed results are not sensitive to the choice of method, whether based on the CCA, SVD, or empirical orthogonal function (EOF) decompositions. In this chapter, the post-processing procedures of error correction are developed based on the SVD analysis and a pointwise statistical downscaling method. By comparing the potential predictabilities with and without

the correction, we can evaluate how the post-processing of error correction enhances predictability in the regions of interest.

At present, dynamical seasonal prediction procedures are categorized as tier-2 and tier-1 systems. The tier-2 system treats the atmosphere and the ocean (specifically SST) separately. This system relies on an AGCM integrated with a prescribed (either observed or predicted) SST boundary condition and atmospheric initial condition. The potential predictability of tier-2 systems have been examined internationally by the Seasonal Model Intercomparison Project (SMIP II) initiated by the Climate Variability and Predictability Program (CLIVAR)/Working Group on Seasonal to Interannual Prediction (WGSIP). The purpose of SMIP II is to evaluate the current dynamical seasonal prediction systems within a framework in which the lower boundary conditions are prescribed from the observed SSTs for the 20 years between 1979–1998. On the other hand, SMIP/Historical Forecast Project (HFP) uses predicted SST conditions instead of past observations, and therefore the SMIP/HFP evaluates the real seasonal predictability of current operational prediction systems.

The tier-1 system utilizes a coupled ocean–atmosphere model. At present, the climatology of coupled models has a large systematic bias. However, as mentioned before, the coupled model has some advantages in simulating monsoon anomalies, particularly in the subtropical western Pacific and Indian Oceans, where air–sea interaction plays an important role in producing seasonal mean anomalies. Recently, the European community has established the DEMETER based on the seven coupled models used in European countries (Palmer *et al.*, 2004). The aim of DEMETER is to develop a multimodel tier-1 seasonal prediction system and evaluate the skill of the prediction system. At present the European Centre for Medium-Range Weather Forecasts (ECMWF) produces a regular seasonal prediction based on the DEMETER. This chapter also shows the capability of the tier-1 DEMETER system.

Section 15.2 describes a prediction experiment and the data utilized in the present chapter. The potential predictabilities of tier-2 systems are examined in terms of the signal-to-noise ratio in Section 15.3, and in terms of anomaly correlation in Section 15.4. The potential predictability is defined here as the predictability obtained by prescribing the observed (not predicted) SST boundary conditions in the model. Section 15.5 introduces a statistical correction method and shows how the prediction skill is improved after the correction. Section 15.6 shows the potential predictability of various multimodel ensemble prediction systems. In contrast to the potential predictability examined in the previous sections, real predictabilities are assessed in Section 15.7 using a tier-2 system with predicted SSTs and tier-1 systems (DEMETER coupled models). Summary and concluding remarks are given in Section 15.8.

## 15.2 MODELS AND EXPERIMENT

The data utilized in the present study have been obtained from the APCN. The APCN aims to produce and disseminate a multimodel ensemble seasonal prediction

**Table 15.1.** Description of the five models used in the present study.

| Institute | Resolution | | Physical parameterizations |
|---|---|---|---|
| JMA | T63L40 | Convection | Prognostic Arakawa–Schubert scheme (JMA, 2002) |
| | | Radiation | JMA (2002) |
| | | Land surface | Simple Biosphere Model (Sellers *et al.*, 1986) |
| KMA | T106L21 | Convection | Kuo scheme (Kuo, 1974) |
| | | Radiation | Lacis and Hansen (1974) |
| | | Land surface | Simple Biosphere Model (Sellers *et al.*, 1986) |
| NASA | $2^\circ \times 2.5^\circ$L34 | Convection | Relaxed Arakawa–Schubert scheme (Moorthi and Suarez, 1992) |
| | | Radiation | Chou and Suarez (1994, 1996) |
| | | Land surface | Mosaic LSM (Koster and Suarez, 1992) |
| NCEP | T62L28 | Convection | Relaxed Arakawa–Schubert scheme (Moorthi and Suarez, 1992) |
| | | Radiation | Chou (1992) and Chou and Suarez (1996) |
| | | Land surface | OSU two-layer model (Pan and Mahrt, 1987) |
| SNUT | 63L21 | Convection | Relaxed Arakawa–Schubert scheme (Moorthi and Suarez, 1992) |
| | | Radiation | 2-stream k-distribution scheme (Nakajima and Tanaka, 1986) |
| | | Land surface | NCAR LSM (Bonan, 1995) |

based on operational prediction products of APEC member countries. Among the products used are the dynamical seasonal prediction data produced by the Japan Meteorological Agency (JMA), Korea Meteorological Administration (KMA), National Aeronautical Space Agency (NASA), National Centers for Environment Prediction (NCEP), and Seoul National University (SNU), as part of SMIP II, led by the CLIVAR WGSIP. The observed SSTs are prescribed for integration. Therefore, the SMIP II can estimate the upper bound of seasonal predictability but not the actual predictability. The initial conditions are obtained from their own initialization scheme or the NCEP reanalysis data. See the details of SMIP II on *http://www-pcmdi.llnl.gov/projects/smip/smip2.php*. The above models consist of different combinations of physical parameterizations, listed and summarized in Table 15.1. The DEMETER data has also been used in the present study. Details of DEMETER can be found in Palmer *et al.* (2004) and the participating models of DEMETER are listed in Table 15.2.

The present study focuses on the predictability of seasonal mean rainfall for boreal summer. For brevity, hereafter 'boreal summer' is abbreviated to 'summer'. The prediction data of each model consists of 10 member predictions of summer mean precipitation for the 21 summers of 1979–1999, except the NASA and JMA models, consisting of 9 and 6 members, respectively. The 10 members were generated with the observed initial conditions at 00:00 Z and 12:00 Z 27–31 May. The horizontal resolution of all data is converted to $2.5^\circ$ in longitude and $2.5^\circ$ in latitude. Since

**Table 15.2.** Brief description of the seven ocean–atmosphere coupled models of DEMETER.

| Institute | AGCM | Resolution | OGCM | Resolution |
|---|---|---|---|---|
| CERFACS | ARPEGE | T63<br>31 levels | OPA 8.2 | $2.0 \times 2.0$<br>31 levels |
| ECMWF | IFS | T95<br>40 levels | HOPE-E | $1.4 \times 0.3 - 1.4$<br>29 levels |
| INGV | ECHAM-4 | T42<br>19 levels | OPA 8.1 | $2.0 \times 0.5 - 1.5$<br>31 levels |
| LODYC | IFS | T95<br>40 levels | OPA 8.2 | $2.0 \times 2.0$<br>31 levels |
| Meteo-France | ARPEGE | T63<br>31 levels | OPA 8.0 | $182GP \times 152GP$<br>31 levels |
| Met Office | HadAM3 | $2.5 \times 3.75$<br>19 levels | GloSea OGCM based on HadCM3 | $1.25 \times 0.3 - 125$ |
| MPI | ECHAM-5 | T42<br>19 levels | MPI-OM1 | $2.5 \times 0.5 - 2.5$<br>23 Levels |

the climatological mean precipitation of each model was presented in Kang *et al.* (2002) and documented elsewhere, we will focus on the deviation (anomaly component) from the 21-year predicted climatology of each model. The anomalies thus obtained do not contain the systematic error of each model climatology. The observed precipitation data for verification is obtained from the Climate Prediction Center Merged Analysis of Precipitation (CMAP) data set (Xie and Arkin, 1997).

## 15.3 LIMIT OF SEASONAL PREDICTABILITY

In this chapter, the interannual variance in model prediction is decomposed into the external (signal) part, related to the SST forcing, and the internal (noise) part, related to the atmospheric non-linear internal dynamics, and the theoretical limit of seasonal predictability is examined in terms of the signal-to-noise ratio. Figure 15.1(a) shows the variance in observed summer mean precipitation for the 21 years. The spatial pattern of Figure 15.1(a) is similar to that of the climatological summer mean shown in Kang *et al.* (2002), indicating that large variability appears in regions of large mean precipitation. Figure 15.1(b–f) are the corresponding variances of each model. Each model variance is estimated based on the predictions of all members for the 21 years, and it will be referred to as the total variance. As in the observation, the spatial distribution of the simulated variance appears to be similar to that of the corresponding climatological mean. However, the magnitudes of the simulated variances are quite different for different models. The NCEP variance is particularly large and about 10 times larger than that of the JMA over Indo-China, south China, and Indian regions. The NCEP model has much larger interannual variances than those actually observed, and the JMA model has much less variance in most of the

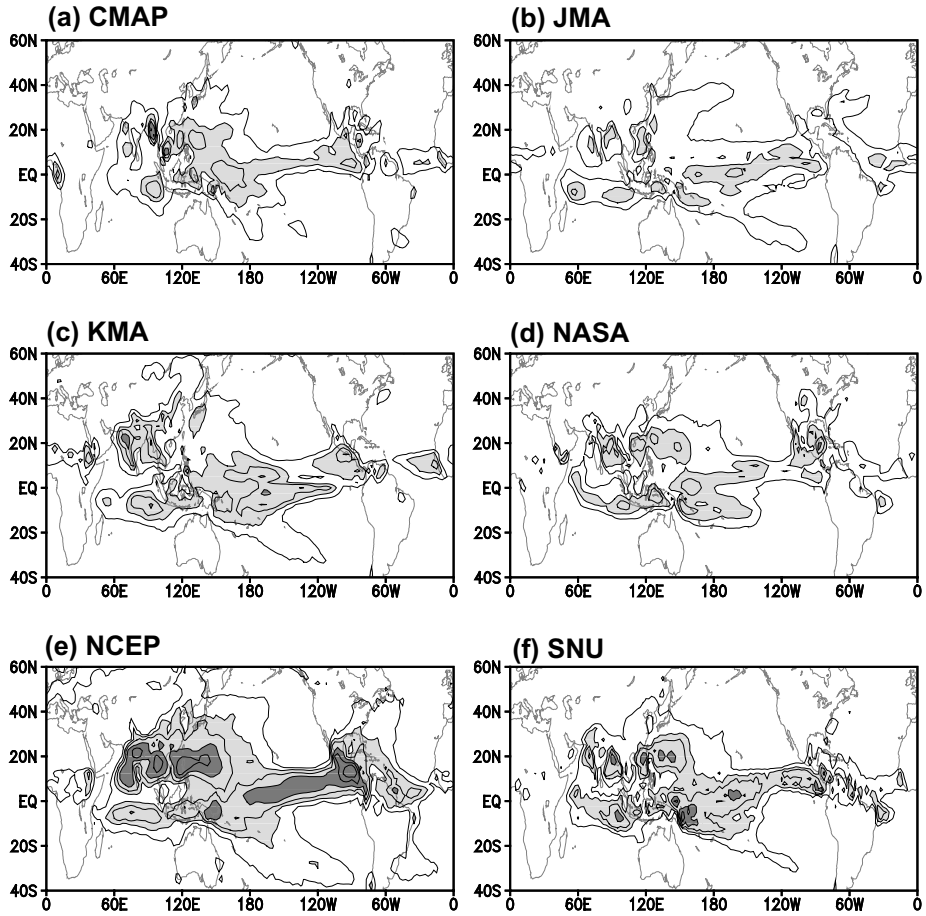


**Figure 15.1.** Variances of summer mean precipitation anomalies for the 21-year period (1979–1999). (a) CMAP observation precipitation, (b) JMA, (c) KMA, (d) NASA, (e) NCEP, and (f) SNU prediction models. The variance of each model is computed using all the ensemble members of the 21-year predictions. The contour interval is 1, 3, 6, 12, 24, and 48 $mm^2\,day^{-2}$ and light and dark shadings indicate a variance of more than 3 and 12 $mm^2\,day^{-2}$, respectively.

regions, particularly over the Asian monsoon region. The difference among the model variances is partly related to the difference in the mean climatology and to the different combinations of model physics. But, it is difficult to identify the model physics responsible for generating such large differences.

The total variance ($\sigma^2_{TOT}$) is divided into the external ($\sigma^2_{SST}$) and internal variances ($\sigma^2_{INR}$; Rowell, 1998). The ensemble mean is considered to be the external component of the prediction forced by the SST forcing, and the deviation from the ensemble mean is the stochastic internal component of the prediction. The

internal variance can then be expressed as:

$$\sigma_{INR}^2 = \frac{1}{N(n-1)} \sum_{i=1}^{N} \sum_{j=1}^{n} (x_{ij} - \overline{x_i})^2 \tag{15.1}$$

where $x$ is the precipitation, $i$ indicates the individual year, $N = 21$, $j$ is the ensemble member, and $n$ is 6 to 10 for different models. $\bar{x}_i$ is the ensemble mean. The external variance is obtained by the mean square of the deviation of each year's ensemble mean from the climatological mean and with a consideration of bias correction, as in Rowell (1998):

$$\sigma_{SST}^2 = \sigma_{EN}^2 - \frac{1}{n}\sigma_{INR}^2 \quad \text{and} \quad \sigma_{EN}^2 = \frac{1}{N-1} \sum_{i=1}^{N} (\overline{x_i} - \overline{\overline{x}})^2 \tag{15.2}$$

where $\overline{\overline{x}}$ is the climatological mean and $\overline{\overline{x}} = 1/(Nn) \sum_{i=1}^{N} \sum_{j=1}^{n} x_{ij}$. It should be noted that the sum of external and internal variances expressed above is equal to the total variance.

Figure 15.2(a–e) show the external variances of various models, and Figure 15.2(f–j) the internal variances. The signal-to-noise ratio, the ratio of the external part to the internal part of the corresponding model, is shown in Figure 15.2(k–o). All the models produce large external variances over the tropical oceans that are much larger than the internal variance of the same model, particularly the ENSO region. This result indicates that tropical rainfall is less controlled by atmospheric internal processes and is thus less predictable for a given SST condition. In the extratropics, on the other hand, the internal variances are bigger than the external variances of the same model (Figures 15.2(k–o)), and therefore the extratropical atmosphere is more controlled by non-linear stochastic processes and less predictable.

Over the Asian monsoon–western Pacific region, the external and internal parts appear to be equally important for all models, although some models (JMA, NASA, and SNU) have relatively large values of the signal-to-noise ratio over the region (Figures 15.2(k–o)) compared with those of the KMA and NCEP models. It is interesting to note that the internal variance is generally proportional to the external variance. In particular, the large variance of the NCEP model shown in Figure 15.1 is partly due to a large internal variance, particularly over the Asian monsoon region. On the other hand, the internal variance of the JMA model is very weak. As a result, the JMA model has relatively large values of signal-to-noise ratio, although its forced variance is significantly weaker than those of the other models. It should also be noted that the internal variance is very model dependent, indicating that the internal variations are not only controlled by the dynamics but also by the model's physics.

Seasonal predictability is limited by the non-linear stochastic processes in the atmosphere, shown in terms of internal variance in Figure 15.2. Therefore, the seasonal prediction could not be perfect even if we had a perfect GCM and perfect boundary conditions and almost perfect initial conditions. Here, the theoretical limit of seasonal predictability is examined by separating the observation

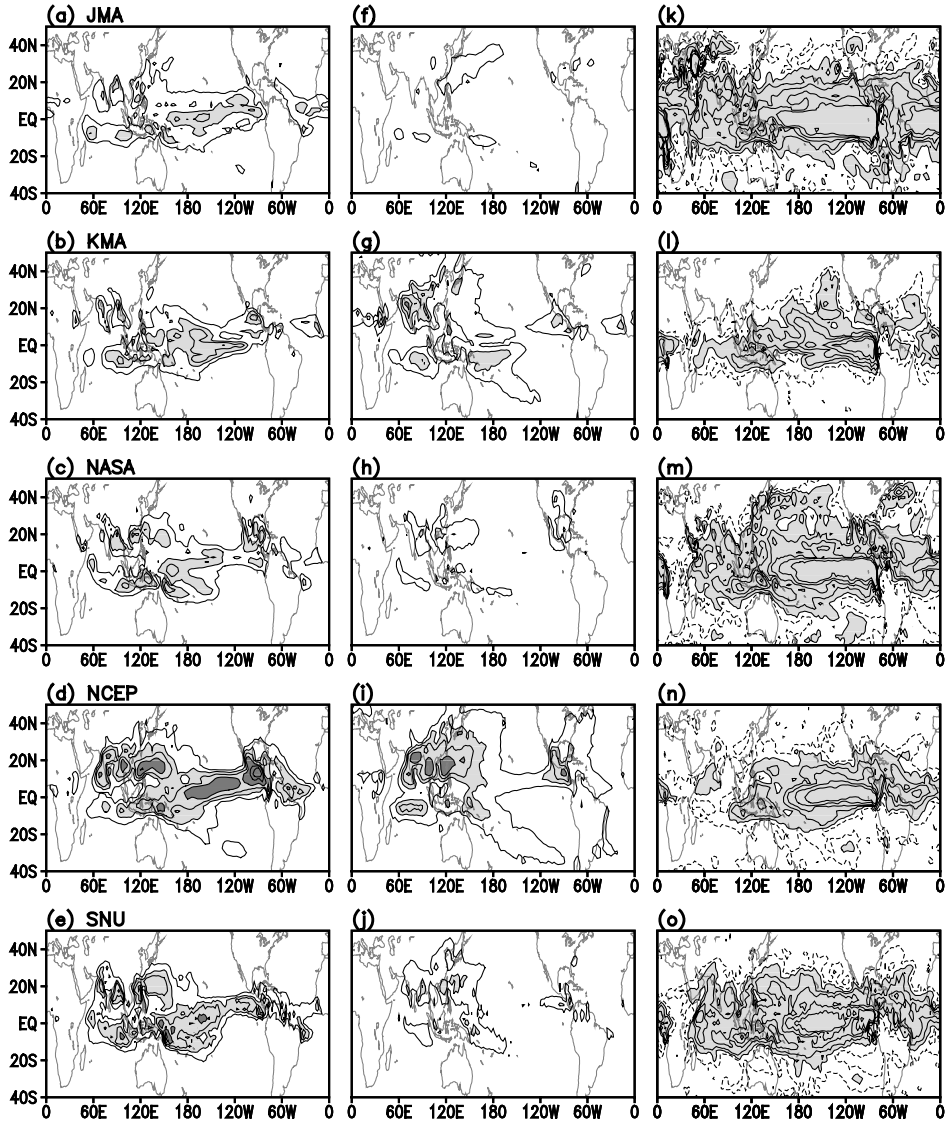


**Figure 15.2.** (a)–(e) External variance of precipitation based on the ensemble average of each year. (f)–(j) Internal variance based on the deviation of individual members from the ensemble average. Contour interval is 1, 3, 6, 12, 24, and 36 $mm^2\,day^{-2}$ and light and dark shadings indicate a variance of more than 3 and 12 $mm^2\,day^{-2}$, respectively. (k)–(o) Signal-to-noise ratio defined by the ratio of the forced variance to the free variance. Contour levels are 1, 2, 4, 8, and 16 and the dashed line indicates 0.5. Shading indicates a signal-to-noise ratio bigger than 1. Each model is marked at the upper left corner of panels (a)–(e).

($x$) into a signal ($x_S$) and noise ($x_N$). The signal is related to the slowly varying boundary conditions. The corresponding model variable is then expressed as $y = y_S + y_N$. Assuming that the model signal is $y_S = \alpha x_S + y_e$ as in Sugi (2004), where $\alpha$ is the linear regression coefficient between $x_S$ and $y_S$, and $y_e$ is the model error. Then, the model variable $y = \alpha x_S + y_e + y_N$. The correlation coefficient between the observation and model variable can be expressed as:

$$R = \frac{\alpha V(x_S)}{V(x)^{1/2}(\alpha^2 V(x_S) + V(y_e) + V(y_N))^{1/2}} \tag{15.3}$$

where $V(x)$ is the variance of $x$. The above equation can be driven by assuming that the signal, noise, and error are independent of each other, and therefore all covariances of $\mathrm{Cov}(x_S, x_N)$, $\mathrm{Cov}(x_S, y_e)$, $\mathrm{Cov}(x_N, y_e)$, $\mathrm{Cov}(y_e, y_N)$, and $\mathrm{Cov}(x_N, y_N)$ are zero. Then the correlation skill can be maximized by minimizing the model error and the noise part. The noise part can be reduced by the ensemble mean procedure – the mean of many predictions with slightly different initial conditions. The model error can be corrected by statistical correlation methods, discussed in Section 15.5, and by using a multimodel composite, discussed in Section 15.6. The theoretical limit of seasonal prediction correlation skill can be expressed as:

$$R_{\mathrm{Limit}} = \sqrt{\frac{V(x_S)}{V(x)}} = \sqrt{\frac{\rho}{\rho + 1}} \tag{15.4}$$

As in (15.4), the theoretical limit can also be expressed in terms of the signal-to-noise ratio ($\rho$). Figure 15.3(a) shows the distribution of $R_{\mathrm{Limit}}$ estimated using the SNU AGCM. We can also examine the predictability limit using a hypothetical perfect model (a model with no systematic error). The correlation skill of the perfect model is usually estimated by considering one of the ensemble members as observation and correlating the member with the ensemble mean of the other members. Figure 15.3(b) shows the distribution of perfect model correlation as estimated with the SNU AGCM. As seen in the figure, the theoretical limit of correlation skill is very similar to the perfect model correlation. The relatively small amplitude of perfect model correlation in the extratropics is due to the sampling error associated with an insufficient number of ensemble members. The zonal means of predictability limits of various models are shown in Figure 15.4. The figure indicates that the predictability limit in the tropics is relatively high (correlation skill of about 0.8–0.9), but it rapidly drops in the subtropics near 30°N and is fairly low in the extratropics and polar regions (correlation of about 0.2–0.4). These correlation values are the upper limit of the dynamical seasonal prediction skill that can be achieved with a perfect model and perfect boundary conditions.

## 15.4 POTENTIAL PREDICTABILITY OF VARIOUS MODELS

The potential predictability, defined as the predictability of the model measured with perfect boundary (observed SST) conditions, should be lower than the theoretical limit because of the incompleteness of the models. The model error is estimated as

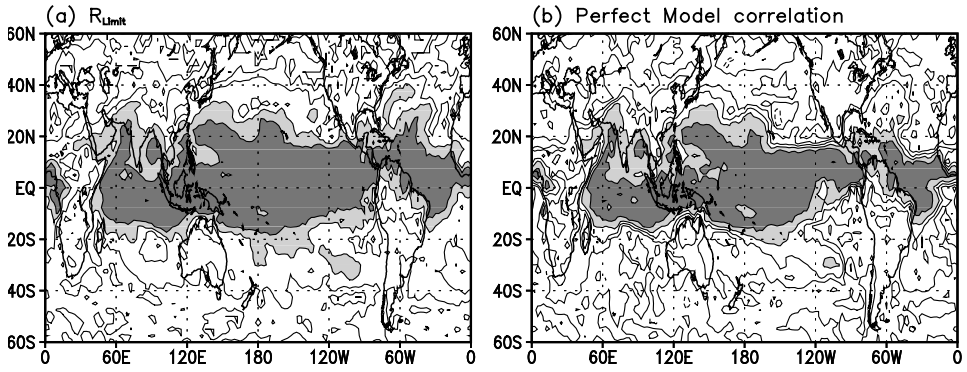


**Figure 15.3.** (a) The spatial distribution of the limit of correlation skill estimated by using the SNU AGCM. (b) Same as in (a) except for the perfect model correlation.

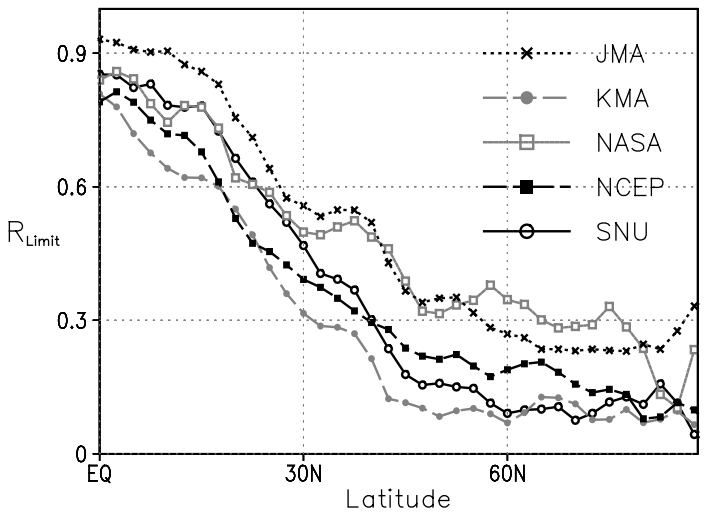


**Figure 15.4.** Zonal mean distribution of theoretical limit of correlation skill for five models in the northern hemisphere. Each line corresponds to each model.

the difference between the ensemble mean of model predictions and the corresponding observations. The error variances of each model are shown in Figure 15.5(a–e). It is interesting to note that the spatial distributions of the errors for all models are similar. All models produce large systematic errors in the Asian monsoon region and along the intertropical convergence zone (ITCZ). The ratio of the external variance to the error variance is shown in Figure 15.5(f–j) for individual models. A ratio exceeding 1 indicates that the prediction signal can be considered to be larger than the error. In the Asian monsoon and western Pacific, all the models produce errors

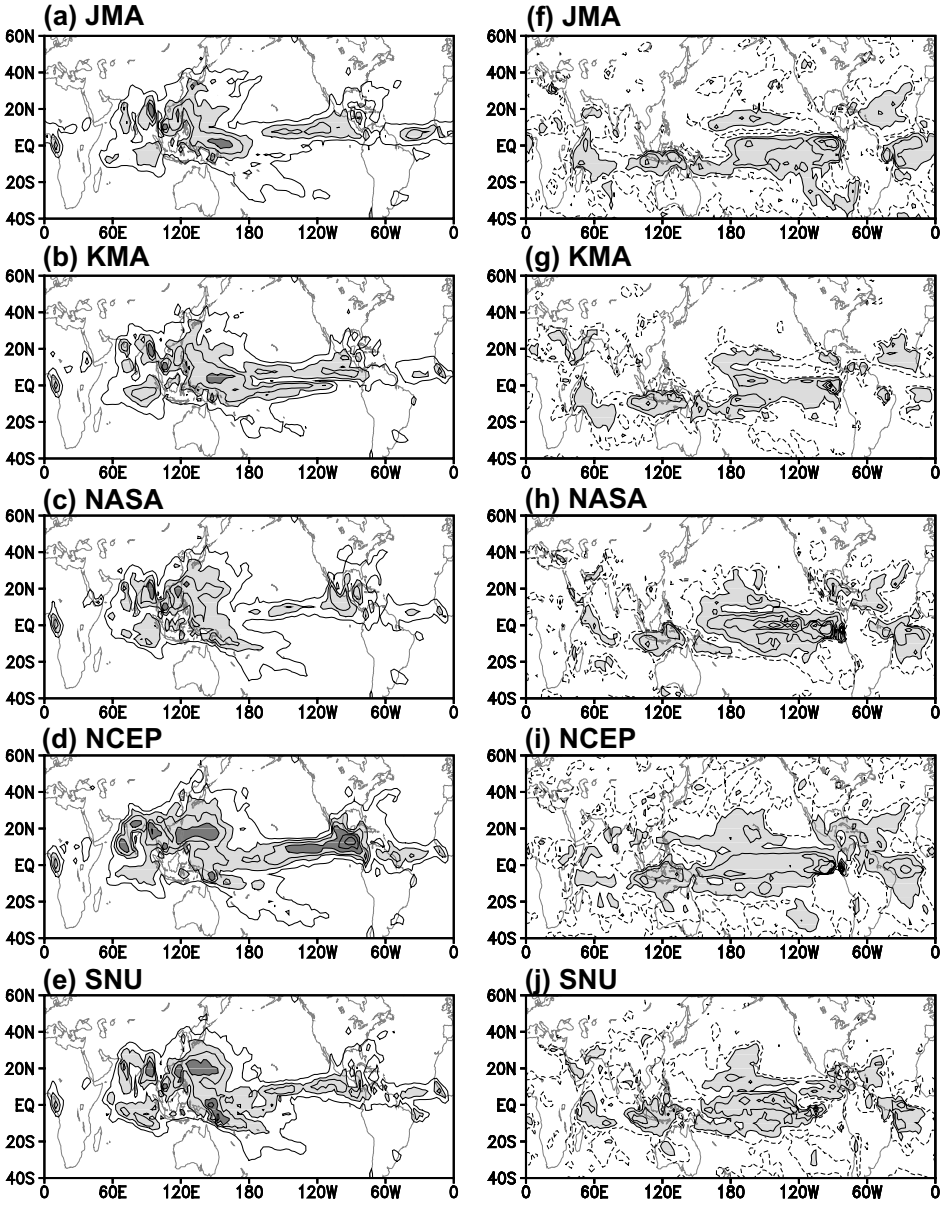


**Figure 15.5.** (a)–(e) Variance of the systematic error – the difference between the ensemble average of prediction and the corresponding observation. Contour interval is 1, 3, 6, 12, 24, and 36 $mm^2\,day^{-2}$ and light and dark shadings indicate a variance of more than 3 and 12 $mm^2\,day^{-2}$, respectively. (f)–(j) Ratio between the variances of ensemble mean and systematic error. Contour levels are 1, 2, 4, and 8 and the dashed line indicates 0.5. Shadings indicates a ratio bigger than 1. Model identification is marked at the upper left corner of each panel.

which are bigger than the signals. This result indicates that the large prediction signals in the monsoon region are biased by the poor performance of the models. In the next section, we investigate whether it is possible to make a reliable monsoon prediction, if the systematic errors are corrected.

The prediction skill of each model is measured by using the correlation between the anomalies of the ensemble mean predictions and the observations for 21 years. Since the observed SST was prescribed in the hindcast predictions, this prediction skill is a measure of potential predictability. Figure 15.6 (color section) shows the global distribution of correlation coefficients between the observed and predicted ensemble mean precipitation at each grid point for the 21 summers. The correlations of various models are shown in Figure 15.6(b–f), and Figure 15.6(a) shows the correlations between observations and the composite of five models. As expected from the previous section, all the models show a large correlation over the ENSO region, where the external (forced) variance exceeds the internal variance and the model error variance. By contrast, over the monsoon region, the correlation skill is very poor for all models. It should be noted that the model composite does not help improve the correlation skill. In the subtropical western Pacific and the Atlantic Ocean, all the models and the composite have large negative correlation values. The negative correlation in the western Pacific is due to model bias, whereas the external response has large systematic errors (Figure 15.5). Recently, Wang *et al.* (2004a) suggested that the poor simulations of precipitation over the western Pacific are due to the tier-2 prediction system, in which atmospheric feedback to the ocean does not exist. This provides additional evidence that ocean–atmosphere coupled processes are important for the summer precipitation anomalies in the western Pacific.

The spatial correlation over the monsoon region (40°–160°E, 20°S–30°N) between the anomalies of the ensemble mean seasonal prediction and the corresponding observed precipitation at each year is shown in Figure 15.7. With a few exceptions, all the models predict the monsoon precipitation poorly for most of the summers. The model composite shows correlation values below 0.3 for most of the summers, except the years 1981, 1986, and 1987. To examine the SST impact on monsoon prediction, the SSTs are averaged for the four cases of good prediction (the years 1981, 1986, 1987, and 1990) and for the cases of bad prediction (the years 1980, 1982, 1994, and 1997). The averaged SST anomalies are shown in Figure 15.8. Comparison between Figure 15.8(a) and (b) clearly demonstrate that monsoon precipitation is indeed closely related to SST anomalies, particularly over the oceans surrounding the Asian monsoon region and the eastern tropical Pacific.

## 15.5 PREDICTION SKILL AFTER ERROR CORRECTION

### 15.5.1 Error correction and verification methods

The model bias in the external component appears in a systematic way, in both the climatological mean and the anomaly component. The mean bias can be corrected

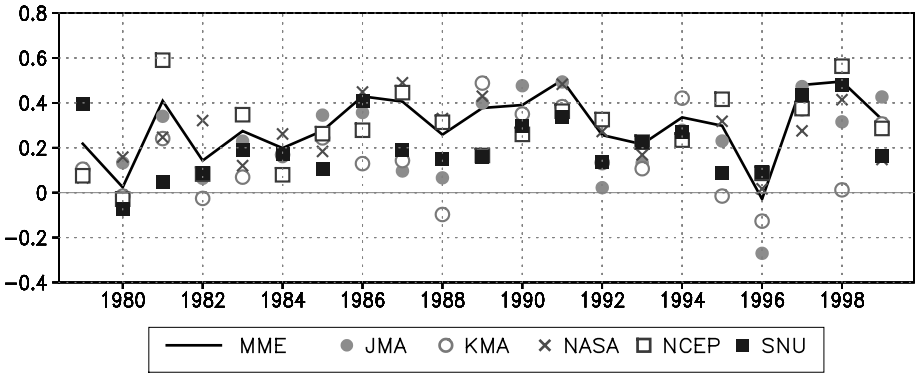


**Figure 15.7.** Pattern correlation coefficients between the observed and predicted precipitation over the monsoon region (40°–160°E, 20°S–30°N). Correlation values of each model and model composite are shown by various marks denoted in the figure.

by subtracting the predicted climatology from the prediction for an individual year. The systematic error of the anomaly component is related to the incorrect performance of the GCM in simulating the anomalies, predominantly forced by the SST anomalies. It should be noted that a slight shift in the spatial pattern of the model anomaly can result in a substantial drop in skill scores when the skill is measured based on the performance at individual grid points. Here, two statistical correction methods are introduced. The first method is based on the SVD (Ward and Navara, 1997; Feddersen *et al.*, 1999; Kang *et al.*, 2004). As in Kang *et al.* (2004), the systematic errors of the predicted anomaly are corrected by replacing the SVD modes of prediction by the corresponding observed modes. The transfer function for the replacement can be constructed as follows:

$$X(x,t) = \sum_{i=1}^{P} \alpha_i Y_i(t) R_i(x) \tag{15.5}$$

where $X(x,t)$ is the corrected field; $Y(t)$ is the time coefficient of the SVD mode for the predicted field; $R(x)$ is the projection of the SVD singular vector onto the observed field; $i$ is the mode number; $P$ the total number of the SVD modes; and $\alpha$ is the correlation coefficient between the time series of the SVD mode of prediction and the corresponding SVD time series of observations. It should be noted that before obtaining the SVD modes, the EOF analysis is applied to the predicted and observed anomalies separately, and the observed and predicted fields are reconstructed by retaining the leading 10 EOF modes of each field. This process filters out small-scale anomalies and smoothes the spatial fields.

It should be noted that the SVD-based correction method can not correct a bias which is not related to leading SVD modes and/or has a local character. Another correction method, used in this chapter, is the so-called 'point-wise downscaling (PDS)' method which is based on the large-scale patterns of model variables

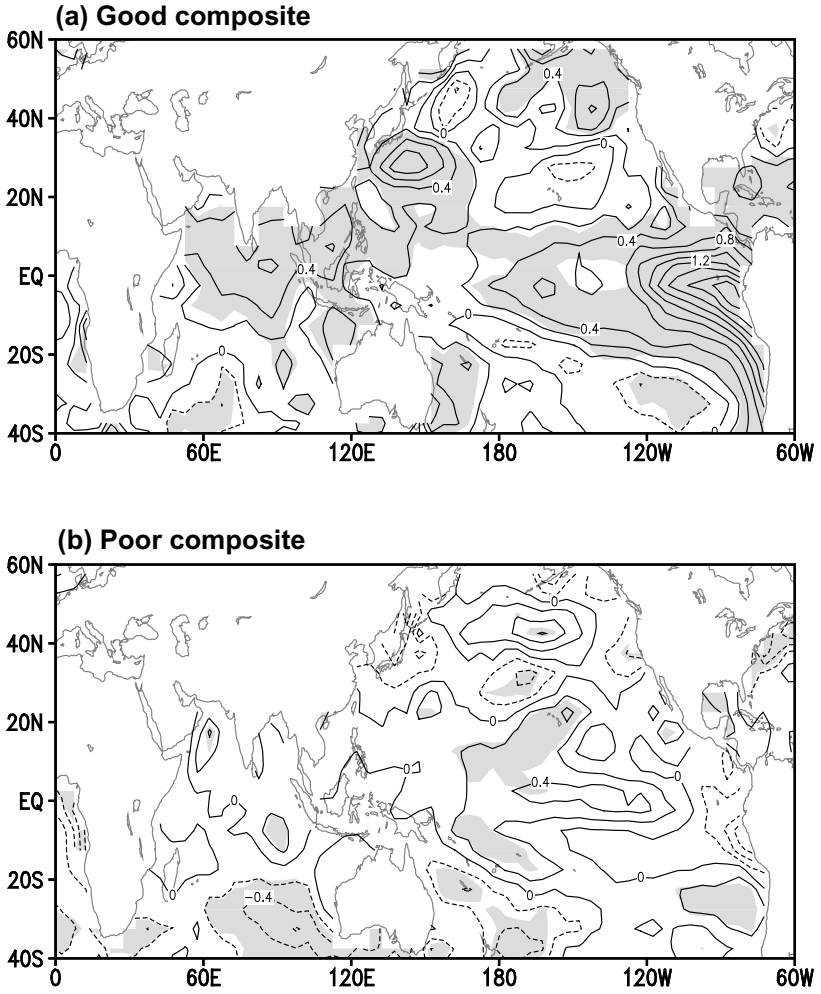


**Figure 15.8.** (a) Composite SST anomalies for the years of good monsoon prediction (1991, 1997, and 1998). (b) Those for the years of poor monsoon prediction (1980, 1982, and 1996). Selected cases exceeding one standard deviation of the correlation coefficient of a composite prediction are shown as solid lines in Figure 15.6(b). Shadings denote the anomalies that are significant at the 99% level of each grid point (Student t-test).

correlated to local (grid point) observed precipitation. Once the model patterns have been determined from hindcast prediction data, the local precipitation can be predicted by a linear combination of the predictors obtained by projecting the patterns onto the dynamical prediction data. The idea of PDS is similar to statistical prediction using indices of large-scale patterns. The detailed procedure is as follows.

Suppose the predictand and predictor field are $Y(t)$ and $X(\lambda, \phi, t)$, respectively. Here $Y$ is a local observed precipitation and $X$ model predicted variables. $\lambda$ and $\phi$

are longitude and latitude, respectively. The spatial pattern of the predictor field associated with the predictand can be expressed as:

$$C(\lambda, \phi) = \overline{Y(t)X(\lambda, \phi, t)} \tag{15.6}$$

and

$$\hat{C}_i = CW_i \quad W_i(\lambda, \phi) = \begin{cases} 1 & \text{inside window} \\ 0 & \text{outside window} \end{cases}$$

The overbar denotes the time mean for the hindcast period. The window $W$ specifies the positions of the spatial patterns of the predictor field. Having obtained the patterns ($\hat{C}_i$), a local predictand (the corrected prediction) can be obtained by projecting the patterns to the predictor variables of the model predicted data, as in the following equation:

$$Y_C(t) = \frac{1}{k}\sum_{i}^{k}\left(a_i\left\{\sum_{\lambda,\phi} C(\lambda, \phi)W_i(\lambda, \phi) \times X(\lambda, \phi, t)\right\} + b_i\right) \tag{15.7}$$

The regression coefficients $(a, b)$ are obtained by minimizing the error variance of $Y$ using the hindcast prediction data. By applying this technique in a cross-validative manner, one can obtain an independently corrected forecast ($Y_i(t)$) for a particular $i$th window. The most important procedure of the PDS method is the selection of optimal windows. For this purpose, we generate a large number of corrected predictions corresponding to the windows by moving the position and changing the size. The window sizes changed are from 30° longitude × 20° latitude (the minimum size) to 120° longitude × 50° latitude (the maximum size). The optimal windows are selected by comparing the temporal correlation skill of corrected forecasts for corresponding windows with a double cross-validation procedure (Kaas *et al.*, 1996). The final corrected forecast is not determined by a single pattern with the highest cross-validated correlation skill but the ensemble mean of several corrections with several different patterns. The correlation coefficient of each pattern is divided into several categories based on the statistical significance of the correlation between observation and corrected forecasts. We use 6 categories whose lower bounds of significance level are 99.9%, 99%, 97%, 95%, 92.5%, and 90%. Among the 6 categories, only the patterns in the category with the highest significance level are used. If there are five patterns in the first category, the final correction is made by the composite of five corrections based on those patterns. In this case, $k = 5$ in equation (15.7). If there is no pattern in the first category then the patterns of the next category are used, and so on. For the correction of predicted precipitation, the predictor variables used here are precipitation and 850-hPa temperature.

It should be noted that the corrections of prediction toward observation, based on both the SVD and PDS methods, lead to a loss of variability in absolute magnitude. Thus, it may be necessary to apply some sort of inflation [method] to the adjusted field. The most common method of inflation is to multiply the adjusted values by the ratio between the standard deviation of the observations and that of the adjusted values. In the present study, the inflation factor has been obtained by

combining the common method of inflation and the weighting factor considered by Feddersen *et al.* (1999) and used by Kang *et al.* (2004).

### 15.5.2 Predictability after error correction

The error correction method introduced above has been applied to the SNU predictions here, and the applicability of the method to seasonal prediction is examined based on this single model's results. It has then been applied to the other models in the next section. Before making the correction, we examined how well the SNU model reproduces the EOF modes of precipitation variability over the globe. Figure 15.9(a) shows the first eigenvector of observed summer mean precipitation, which explains 24.3% of the total variance, and Figure 15.9(c) is the predicted counterpart, explaining 39.0% of the total variance. Both figures are characterized by an east–west seesaw pattern between the anomalies in the tropical central Pacific and Indonesian subcontinent, although the model centers are shifted to the east. Other noticeable differences include sign differences in the subtropical western Pacific and the Indian Ocean eastward of 60°E. The poor performance of the model in those regions has already been mentioned in the previous section. The time series associated with the eigenvectors, shown in Figure 15.9(e), vary in a similar way and are related to El Niño/Southern Oscillation (ENSO) SST anomalies. The difference between the model and observed eigenvectors in the subtropical western Pacific and Indian Ocean is due to a failure of the model to simulate the responses of ENSO SST anomalies.

The second eigenvector of the observed summer mean precipitation, shown in Figure 15.9(b), explains 15.7% of the total variance. The model counterpart, shown in Figure 15.9(d), shows that the model reproduces the western Pacific center but with a much weaker amplitude. It also produces anomalies in other regions in the Pacific and Indian Ocean that are somewhat different from observation. However, the similarity between the time series associated with observed EOF modes and the corresponding time series of predicted modes provides hope for error correction in the predicted field. The error correction has been completed using equation (15.5) and the SVD modes. The two leading SVD singular vectors (not shown) are very similar to the corresponding EOF eigenvectors shown in Figure 15.9. This similarity could be expected from Figures 15.9(e) and (f), where the two time series of the observed and predicted modes vary almost simultaneously, indicating that the two EOF modes are coupled to each other. The first four SVD modes are used for the correction. The fifth and higher modes consist of small-scale patterns and explain a small fraction of the variance. The sum of the four modes accounts for 41.2% of the total variance.

Figure 15.10(a) shows the spatial distribution of the correlation coefficient between observations and the corrected seasonal predictions based on the SVD method. The correlation coefficients of corrected predictions are replaced by those without correction, if the former is smaller than the latter. Those locations are in the central tropical Pacific, where the correlation coefficient of the original prediction

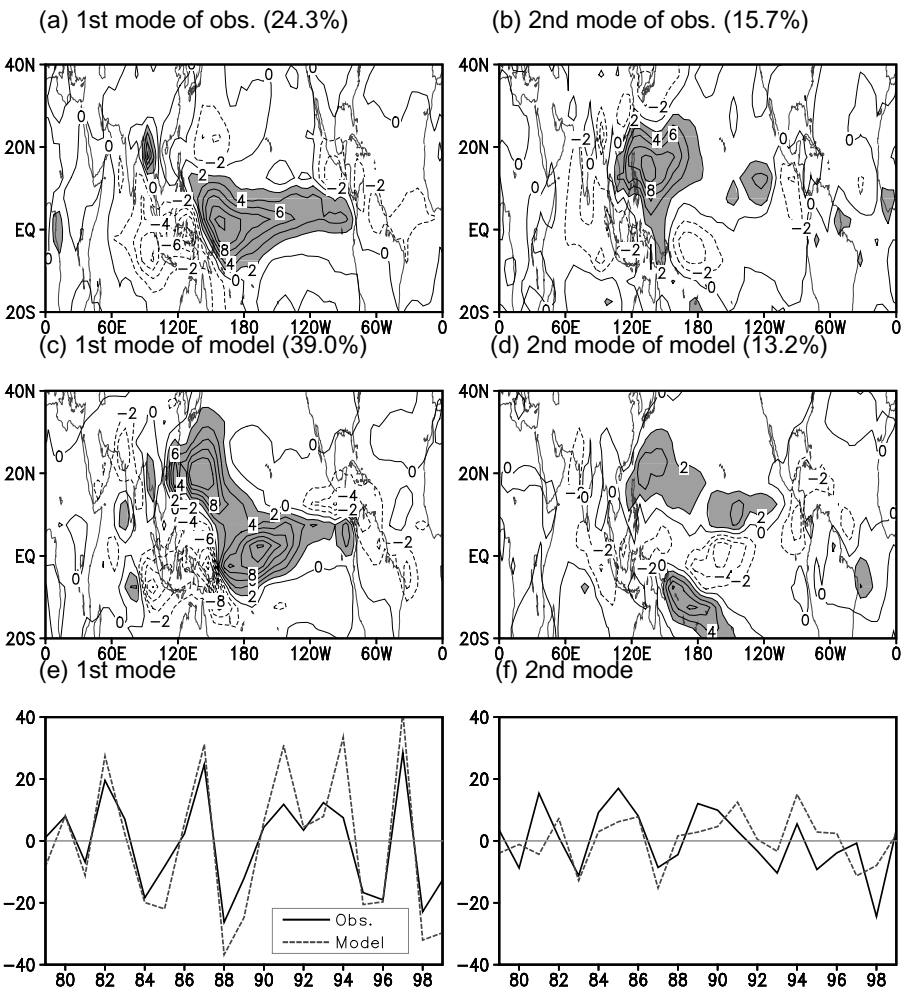


**Figure 15.9.** EOF modes of the observed and simulated ensemble mean precipitation. (a) and (b) are the observed first and second eigenvectors and (c) and (d) the simulated counter parts. (e) and (f) are the time series associated with the eigenvectors. Solid and dashed lines indicate the observed and simulated time series, respectively.

(Figure 15.3) is already very large. Clearly, in most of the regions, the predictability is greatly enhanced by statistical correction. The enhancement of predictability is particularly pronounced in the western Pacific where the prediction skill is negative without correction (Figure 15.5(f)) but has relatively large positive values after correction. The correlation skill of the corrected prediction based on PDS is shown in Figure 15.10(b). The double cross-validation procedure is applied to obtain the correlation skill. In the tropics, both correction methods produce similar results. In the subtropics and extratropics, however, the PDS method has a superior ability to correct errors, particularly in the western Pacific.

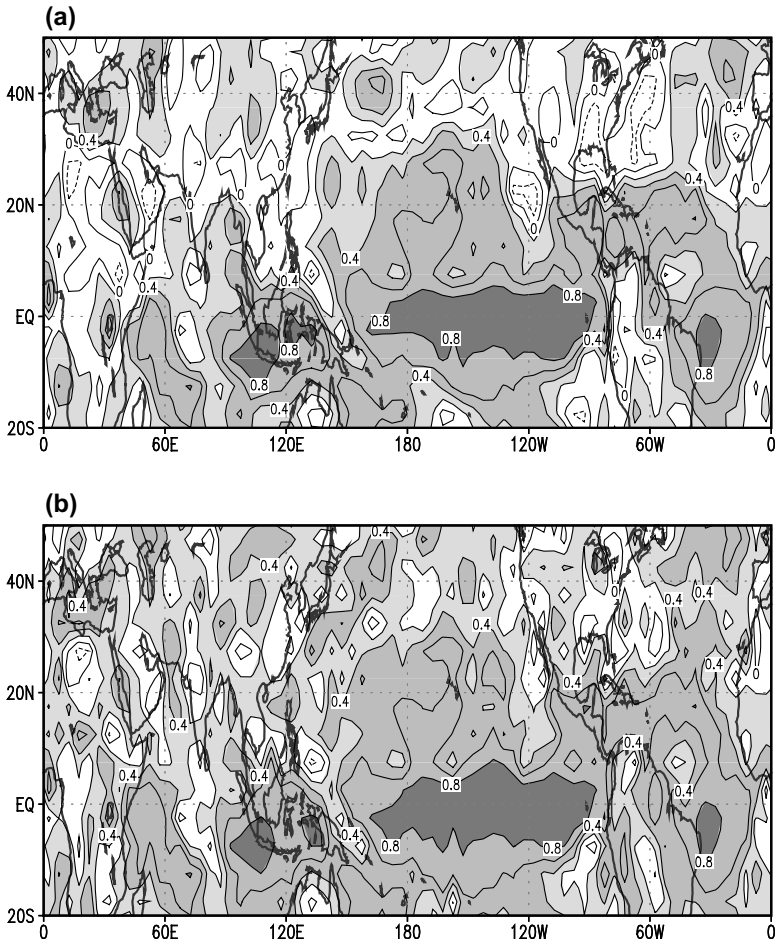


**Figure 15.10.** As in Figure 15.5 except the predicted precipitation of the SNU SMIP after correction of the systematic error using (a) SVD and (b) PDS.

The prediction skill of monsoon precipitation is shown in Figure 15.11 in terms of the spatial pattern correlation between the observed and predicted fields of each year for the monsoon domain of 20°S–30°N and 40°–160°E. In the figure, the open bar indicates the pattern of correlations without correction, and the shaded and black bars indicate those with the corrections based on the SVD and PDS methods, respectively. The predictability is greatly enhanced by the corrections for most of the years. The 21-year averages of correlation values are 0.24 for the prediction without correction, and 0.37 and 0.42 for the predictions with the SVD and PDS correction methods, respectively. Since the PDS method exhibits a better performance than the SVD method, hereafter all corrections are made based on the PDS method.

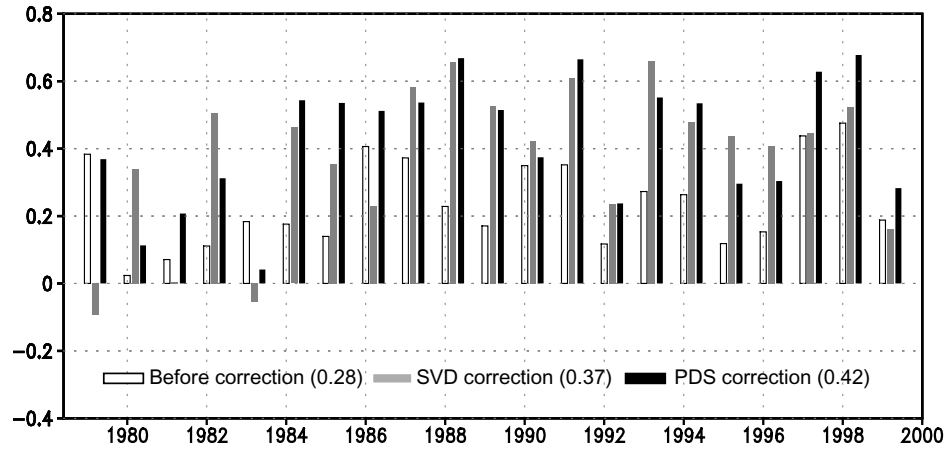


**Figure 15.11.** Pattern correlation coefficients between the observed and predicted precipitations of the SNU SMIP before (open bar) and after the bias correction by the SVD (gray shaded bar) and PDS (black shaded bar) over the monsoon region (40°–160°E, 20°–30°N).

## 15.6 MULTIMODEL POTENTIAL PREDICTABILITY

There are several ways of combining the multimodel outputs. The simplest way is a composite. The basic idea of a multimodel composite is that the errors of the individual models can cancel each other out. However, the multimodel composite may not be necessarily better than the best single model. The superiority condition of the multimodel composite to the best simple model is given here. After normalizing all anomalies with respect to their corresponding variance, the skill score $S$ (here defined as $S = 1 - (V(error)/V(obs))$ can be expressed as:

$$\left.\begin{aligned} S_S &= 2R - 1 \\ S_M &= 2R_M - r_M \end{aligned}\right\} \tag{15.8}$$

Where $S_S$ is the skill score of a single model and $R$ is a correlation coefficient between the observation and the single model $S_M$ is the skill score of a multimodel composite, $R_M = 1/N \sum_{i=1}^{N} R_i$ is the mean correlation skill of the $N$ models used in the multimodel composite, and $r_M = 1/N^2 \sum_{i=1}^{N} \sum_{j=1}^{N} r_{ij}$ is the mean of inter-model correlations $r_{ij}$. The above equation indicates that the multimodel composite has its best skill when several of the best models are chosen to maximize $R_M$ and the models are least dependent on each other to minimize $r_M$. In reality, the multimodel composite is not necessarily better than the single (best) model, mainly because of the inter-model dependency. The difference in the skills, $D = S_M - S_S$, can then be expressed as:

$$D = (1 - r_M) - 2(R - R_M) \tag{15.9}$$

The multimodel composite is better than a single model if $D$ has a positive value. By

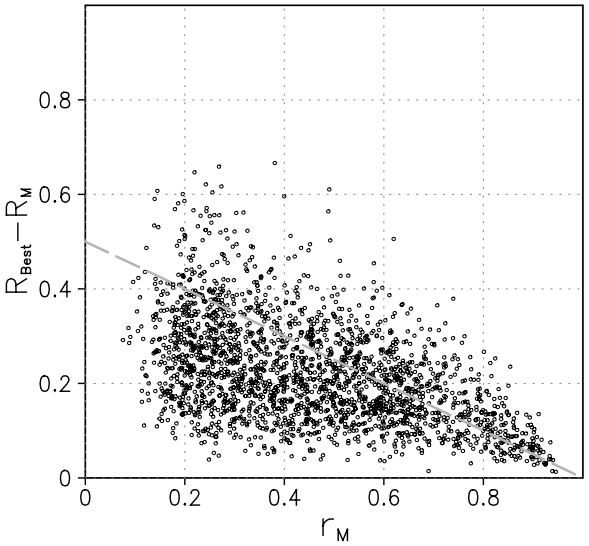


**Figure 15.12.** Distribution of $r_M$ and $R_{\text{Best}} - R_M$, which are computed using five-model precipitation data. Each dot corresponds to each grid point. The thick dashed line indicates the threshold of superiority of the multimodel composite against the single best model. The multimodel composite is better than the single best model below this line.

denoting $R_{\text{Best}}$ as the correlation skill of the best model, $r_M$ and $R_{\text{Best}} - R_M$ at each grid point are computed using the five-model precipitation data – these values are plotted in Figure 15.12. The best model at each grid point is determined by comparing the prediction skills of the five models, obtained based on the 21-year hindcast data. In the figure, the multimodel composite is better than the single best model if the skills of the best model and the multimodel are in the region below the thick line. The figure indicates that the multimodel composite is better than the single best model at most of the grid points, although there are many exceptions.

There are several ways of combining the multimodel outputs other than as a composite. After Krishnamurti *et al.* (1999, 2000a), scientists have tried to improve weather and climate forecasts using an approach called the 'superensemble.' The skill of the superensemble method depends strongly on a post-processing algorithm for the multiple regression of multimodel solutions toward observed fields during a training period. For post-processing, the respective weights for individual models are generated using a multiple regression technique. The conventional superensemble forecast (Krishnamurti *et al.*, 2000a) can be constructed using the following formula.

$$S = \bar{O} + \sum_{i=1}^{N} a_i (F_i - \bar{F}_i) \tag{15.10}$$

Where $F_i$ is the $i$th model forecast, $\bar{F}_i$ is the mean of the $i$th forecast over the training period, $\bar{O}$ is the observed mean over the training period, $a_i$ is the weighting factor of

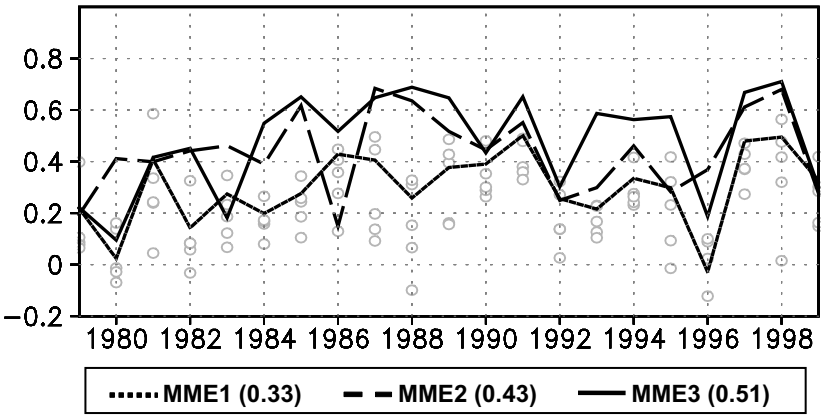


**Figure 15.13.** Time series of the spatial pattern correlations over the monsoon region (40°–160°E, 20°S–30°N) between the observed and the predicted precipitations of MME1 (dotted line), MME2 (dashed line), and MME3 (solid line). MME1, MME2, and MME3 are the multimodel predictions based on a simple composite, SVD based superensemble, and the composite of correction predictions by PDS, respectively. The open gray dots are spatial pattern correlation values of individual models.

the $i$th model, and $N$ is the number of forecast models involved. The design of an optimal weighting function for a long-term forecast is the key to the development of a multimodel superensemble system. Here, the weighting factors are obtained based on the SVD method proposed by Yun *et al.* (2003).

In the present section, the multimodel predictions are a combination of three methods: a simple composite (MME1), the superensemble (MME2), and the composite of model predictions after each model prediction corrected by the statistical PDS method (MME3). It has been mentioned that the superensemble method is also applied to the predictions after error correction. However, the superensemble in this case does not provide better skill compared with the composite of the corrected predictions. This may be because of double fitting to the observation: the first fit of the prediction to the observation for the correction and the second fit for the superensemble.

The spatial pattern correlations over the monsoon region for 1979–1999 were obtained by using MME1, MME2, and MME3, and are plotted in Figure 15.13. As shown in Figure 15.6(b), the composite is not always better than the best individual model prediction, but the average skill of the composite is comparable to that of the best individual model. Therefore, the choice of a multimodel composite prediction will generally be a safe one since we do not know the best model for the prediction. On the other hand, the superensemble skill (MME2) appears, with a few exceptions, to be better than that of the best individual model. However, as shown in the previous section, the prediction skill of individual models after error correction is usually much better than that of the raw prediction. The correlation skill of MME2 appears to be comparable to that of the best individual model after correction. The

composite of corrected predictions (MME3) usually has a superior correlation skill than any of the corrected individual models. The MME3, which is the best system among the prediction systems used here, produces a 21-year average correlation skill of 0.51 for the monsoon summer prediction, which is statistically significant. The correlation skills in other regions and other seasons must be different, and their usefulness should be examined separately. In conclusion, dynamical monsoon seasonal prediction requires a multimodel system with statistical post-processing, which needs further research efforts.

## 15.7 COUPLED MODEL PREDICTABILITY

In the previous sections, seasonal predictability was investigated using AGCM simulations with prescribed observed SST conditions. However, a real operational prediction should use predicted SST as a boundary condition of model integration. The methods of SST prediction currently being used are a persistence model, ocean–atmosphere coupled models, and various statistical models. As indicated in the introduction, however, the tier-2 system (AGCM simulation with prescribed SST) has limits in simulating correctly the atmospheric response to local SST anomalies in the region of active ocean–atmosphere interaction (Wang *et al.*, 2004a). As in Wang *et al.*, the local ocean–atmosphere relationships in the tier-1 and tier-2 systems are examined here, before showing the real seasonal predictability of tier-1 systems.

In contrast to a commonly accepted view that a warmer SST produces more precipitation in the tropics, Wang *et al.* (2004a) showed that observed summer mean precipitation over the tropical western Pacific is negatively correlated with the local SST and atmospheric feedback to the ocean is an important mechanism for determining the western Pacific SST. This atmospheric feedback mechanism is not included in the tier-2 system. As a result, the tier-2 system produces incorrect precipitation anomalies over the western Pacific, as seen in Figure 15.3. Figure 15.14(a) shows the lead-lag relationship (correlation) between the pentad mean rainfall and SST averaged over the western Pacific of 5°–30°N, 110°–150°E for the summer season. The observed relationship, shown with a black line, indicates that rainfall leads the negative SST anomaly with a lead time of about 10 days. Such a relationship may be due to the reduction of solar radiation that comes with more cloud and the increase of surface fluxes associated with an increase of surface wind. This observed relationship is reasonably well simulated with a prototype ocean–atmosphere coupled model – the AGCM coupled with an ocean mixed layer. The mixed layer model used here is a slap model with a fixed 50 m depth and the SST is controlled only by the surface heat fluxes. On the other hand, the tier-2 AGCM simulations show that the rainfall has a weak positive correlation with the SST. The AGCM used for the two experiments is the same (SNU AGCM), and the results strongly suggest the use of an ocean–atmosphere coupled model for the correct prediction of summer rainfall over the western Pacific. We notice that for the winter season, the winter mean precipitation is positively correlated with the SST

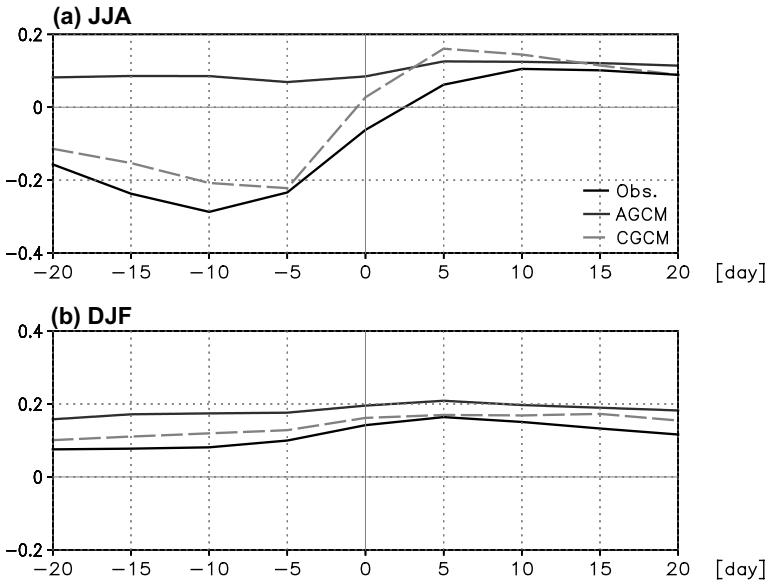


**Figure 15.14.** Lead-lag correlation coefficient between pentad rainfall and SST averaged over the western North Pacific (5°–30°N, 110°–150°E) for June/July/August (*upper panel*; 31–48 annual pentad) and December/January/February (*lower panel*; 1–12 and 68–73 pentad). The black solid line denotes the observed correlation coefficients between pentad CMAP and weekly OISST data during 1982–1999; the dotted line denotes AGCM (1950–1999); and the gray dashed line is for CGCM (25 years), respectively.

and that the tier-2 system can mimic the rainfall–SST relationship in the western Pacific (Figure 15.14(b)). The seasonal dependency of atmosphere–ocean feedback deserves further research.

The local rainfall and SST relationship during the summer was further examined using a fully coupled ocean–atmosphere model and the relationship compared with those of observations and AGCM alone (Figure 15.15, color section). The coupled model used here is the one developed at the Climate Environment System Research Center of SNU which uses the SNU AGCM coupled with a GFDL MOM2 ocean model and the ocean mixed layer model developed by Noh and Kim (1999). Figure 15.15 shows the distribution of local correlation coefficients between the summer mean precipitation and SST at the same grid point for the 21-year observations of 1979–1999 (Figure 15.15(a)), the AMIP AGCM simulation for 1950–1999 (Figure 15.15(b)), and the 25-year simulation of the coupled model (Figure 15.15(c)). Over the ENSO region, all three figures show that the summer mean precipitation is highly positively correlated with local SST, indicating that the atmosphere responds directly to the SST in the region. Over the western tropical Pacific and extratropical Pacific, on the other hand, the observed relationships are well reproduced by the coupled model, but are quite different (having a different sign) from those of the AGCM, again indicating that coupled ocean–atmosphere processes are important for simulating the summer rainfall over the regions.

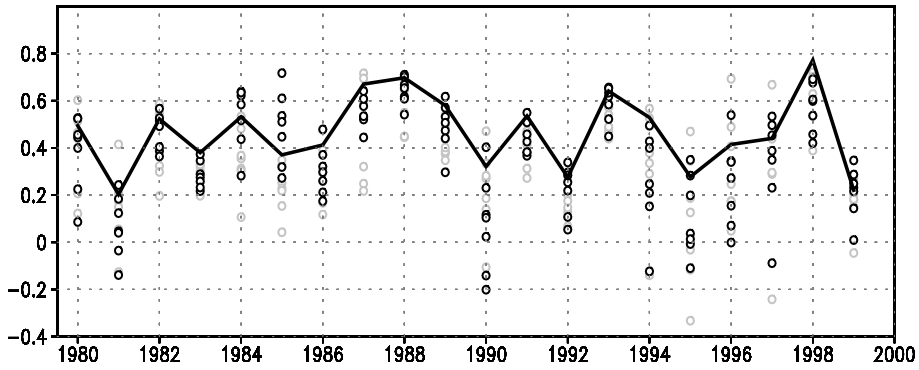


**Figure 15.18.** The interannual variation of the averaged value of pattern correlation of the individual DEMETER models before (gray) and after (black) the bias correction over the monsoon region. The thick solid line is the spatial pattern correlation of the multimodel composite after the correction (MME3).

The coupled model produces precipitation anomalies in a similar manner as observed. But it does not guarantee a high prediction skill, which can be achieved only if its SST prediction is reasonably good. We now examine the prediction skill of tier-1 systems using the seven coupled ocean–atmosphere models participating in the DEMETER project, listed in Table 2. Figure 15.16 (color section) shows the correlation skills of summer mean SST for the individual models and the multimodel ensemble over the globe. All models have a relatively high correlation skill over the tropical Pacific and a relatively low correlation skill in the extratropical oceans. The correlation skill of the multimodel composite, shown in Figure 15.16(a), is higher than those of individual models in most of the regions and is particularly high (over 0.8) in the tropical Pacific. The prediction skills for precipitation of the coupled models, shown in Figure 15.17 (color section), are relatively high in the tropical Pacific but poor in other regions. The skill of the multimodel composite (Figure 15.17(a)) is similar to that of the best model. As expected, the tier-1 systems produce slightly better prediction skills over the western Pacific compared with the negative correlation skills that the tier-2 systems produce in the region.

The year-to-year variations of spatial pattern correlation for the monsoon region, between the predicted and observed precipitation, are shown in Figure 15.18. Shaded and dark circles indicate the correlation values of raw and corrected predictions, respectively. A statistical correction based on the PDS method improves the correlation skill in most cases. The MME3 multimodel ensemble method (composite of the corrected predictions), shown to be the best method among the several multimodel ensemble methods treated in Section 15.5, is now applied to the DEMETER predictions. The solid line in the figure shows year-to-year variations of the spatial pattern correlation between the observed and the MME3 precipitation for the monsoon region. The 21-year average of the MME3

correlation values is 0.47. This value may represent the best prediction skill of summer monsoon precipitation that we can achieve at present.

## 15.8 SUMMARY AND CONCLUDING REMARKS

This chapter reviewed the present status of state-of-the-art dynamical seasonal prediction systems and demonstrated a possible improvement to the predictions based on statistical correction and a combination of several independent predictions. In particular, the seasonal predictability of summer mean precipitation over the Asian monsoon–western Pacific region was assessed by using the 21-year hindcast predictions of five models for 1979–1999. The five models consisted of the operation seasonal prediction models of the Japan Meteorological Agency (JMA), Korea Meteorological Administration (KMA), National Aeronautical Space Agency (NASA), National Centers for Environment Prediction (NCEP), and Seoul National University (SNU). The historical prediction data were produced as part of the CLIVAR/Seasonal Prediction Model Intercomparison Project II (SMIP II). In this experiment, the SST boundary conditions during the prediction period were prescribed with observed SSTs, and thus the potential predictability was assessed. The potential predictabilities of individual models and a multimodel ensemble system were shown by various methods including the signal-to-noise ratio, based on the analysis of variance and anomaly correlations. In addition to the potential predictability of the tier-2 systems, the real seasonal predictabilities of tier-1 systems were examined based on the coupled model predictions of the DEMETER project.

The signal-to-noise ratio of seasonal mean precipitation over the monsoon region is lower than that of other tropical regions. In addition to a lot of noise, all tier-2 models produce large systematic errors in the Asian monsoon region, particularly in the western Pacific. As a result, all models exhibit very poor correlation skill over the monsoon region. The model composite prediction does not help to improve the correlation skill. For the subtropical western Pacific and the Atlantic Ocean, all models and their composites show correlation skills with relatively large negative values. The negative skill in the western Pacific is due to model bias, where the external response has a large systematic error. Recently, Wang *et al.* (2004a) suggested that the poor simulations of precipitation over the western Pacific are due to the tier-2 prediction system, where the atmosphere is forced by the prescribed SST, but in nature the ocean–atmosphere coupled processes are active and atmospheric feedback to the ocean, which is missing in the tier-2 approach, is important in the western Pacific.

To correct the model bias, statistical methods based on the SVD and a PDS method were developed and applied to individual model predictions. It has been shown that statistical correction is effective in enhancing predictability, particularly for the Asian monsoon–Pacific region, where a large model bias is included in the forced signal (Kang *et al.*, 2004). The enhancement of predictability is particularly pronounced in the western Pacific where the correction skill is negative without correction but has relatively large positive values after correction. It has been

shown that point-wise correction is generally better than the correction with leading SVD modes.

The errors of individual models can be reduced by combining them into multimodel predictions. A theoretical case was made for the superiority of a multimodel composite over the single best model. It was shown that the multimodel composite has a good skill when several best models are chosen and the models are least dependent on each other. Intermodel dependency is a crucial problem at present for multimodel prediction, whose performance is better than that of the single best model. The seasonal predictability of multimodel ensemble prediction was assessed by using several multimodel methods including simple composite, superensemble, and composite of corrected individual predictions. It has been shown that a reasonably good dynamical seasonal prediction can be achieved when we use the multimodel composite after applying statistical correction to individual predictions.

The multimodel seasonal prediction based on coupled models was also examined by using the hindcast prediction data of DEMETER. It has been anticipated that the tier-1 system will often produce large systematic errors, particularly in the extratropical region, compared with those of the tier-2 system with the prescribed SST anomalies obtained from the same tier-1 system. However, this study shows that the tier-1 system can predict summer mean precipitation better, particularly over the monsoon–western Pacific region, where the atmosphere–ocean feedback is active. The DEMETER tier-1 systems appear to produce better prediction skills over the globe compared with tier-2 systems with predicted SST (not shown). The spatial correlation skill of the DEMETER MME3 for summer mean precipitation, the best among the multimodel ensemble systems treated in this chapter, is 0.47 over the monsoon region. These values may represent the best summer mean precipitation prediction skills that we can achieve with dynamical prediction models at present.

## 15.9 ACKNOWLEDGEMENTS

The authors would like to express their appreciation to their SNU colleagues and students, Dr. Jong-Sung Kug, Ms. Kyung Jin, Mrs. Jin Ho Yoo, Doo-Young Lee, and Ho-Yong Jeong, and Dr. June-Yi Lee at NASA/GSFC, who contributed their work to the materials presented in this chapter. The present study was supported by the Climate Environment System Research Center at Seoul National University and the Korea Meteorological Administration.